**Reconstitution of DNA Segregation Driven by Assembly of a Prokaryotic Actin Homolog**

Ethan C. Garner, *et al.*
*Science* **315**, 1270 (2007);
DOI: 10.1126/science.1138527

linked to reduced D2 receptor function, specifically because of the presence of the D2 *Taq* I A1 allele (*40, 41*), which has previously been shown by PET to be associated with reduced D2 receptor density in the striatum (*42*).

Our results are consistent with the hypothesis that dysfunctional DA neurotransmission at D2-like receptors in the nucleus accumbens confers susceptibility to increased cocaine self-administration in high-impulsive rats. Recent findings in rhesus monkeys trained to self-administer cocaine support this view (*19, 20*), but there has been little evidence to date that D2 receptor dysregulation that is present either as a trait marker or induced by chronic cocaine exposure is restricted to the nucleus accumbens. Indeed, analogous PET studies in monkeys (*19, 20, 43*) and abstinent human cocaine addicts (*23*) report generalized reductions in D2 receptor availability throughout the striatum. In contrast, as in the present study, D2 receptor density and D2 mRNA content were found to be significantly reduced in the nucleus accumbens but not in the dorsal striatum or medial prefrontal cortex of HR rats (*44*).

The contrast between specific reductions in D2 receptor availability in the nucleus accumbens in rats before cocaine self-administration, as compared to the more divergent effects in the striatum after chronic exposure to cocaine self-administration, suggests the hypothesis that the ventral striatal changes confer susceptibility to cocaine taking, which subsequently affects DA neurotransmission in the dorsal striatum, with corresponding effects on the number of D2 receptors in that region (*20, 23, 43*). Thus, the development of psychostimulant drug addiction may represent a progression from initial impulsivity mediated by the nucleus accumbens to the development of compulsive habitual responding mediated by the dorsal striatum (*32, 45*).

**References and Notes**

1. N. Chakroun, J. Doron, J. Swendsen, *Encephale* **30**, 564 (2004).
2. S. Dawe, N. J. Loxton, *Neurosci. Biobehav. Rev.* **28**, 343 (2004).
3. K. J. Sher, B. D. Bartholow, M. D. Wood, *J. Consult. Clin. Psychol.* **68**, 818 (2000).
4. J. B. Adams et al., *Am. J. Drug Alcohol Abuse* **29**, 691 (2003).
5. K. I. Bolla, R. Rothman, J. L. Cadet, *J. Neuropsychiatry Clin. Neurosci.* **11**, 361 (1999).
6. R. Hester, H. Garavan, *J. Neurosci.* **24**, 11017 (2004).
7. J. D. Jentsch, J. R. Taylor, *Psychopharmacology* **146**, 373 (1999).
8. M. Lyvers, *Exp. Clin. Psychopharmacol.* **8**, 225 (2000).
9. T. A. Paine, H. C. Dringenberg, M. C. Olmstead, *Behav. Brain Res.* **147**, 135 (2003).
10. J. W. Dalley et al., *Psychopharmacology* **182**, 579 (2005).
11. J. W. Dalley et al., *Neuropsychopharmacology* **30**, 525 (2005).
12. P. V. Piazza, J. M. Deminiere, M. Le Moal, H. Simon, *Science* **245**, 1511 (1989).
13. J. R. Mantsch, A. Ho, S. D. Schlussman, M. J. Kreek, *Psychopharmacology* **157**, 31 (2001).
14. E. B. Larson, M. E. Carroll, *Pharmacol. Biochem. Behav.* **82**, 590 (2005).
15. A. D. Morgan, N. K. Dess, M. E. Carroll, *Psychopharmacology* **178**, 41 (2005).
16. B. A. Gosnell, *Psychopharmacology* **149**, 286 (2000).
17. E. L. van der Kam, B. A. Ellenbroek, A. R. Cools, *Neuropharmacology* **48**, 685 (2005).
18. J. L. Perry, E. B. Larson, J. P. German, G. J. Madden, M. E. Carroll, *Psychopharmacology* **178**, 193 (2005).
19. D. Morgan et al., *Nat. Neurosci.* **5**, 169 (2002).
20. M. A. Nader et al., *Nat. Neurosci.* **9**, 1050 (2006).
21. P. V. Piazza et al., *Brain Res.* **567**, 169 (1991).
22. M. Tonissaar, L. Herm, A. Rinken, J. Harro, *Neurosci. Lett.* **403**, 119 (2006).
23. N. D. Volkow et al., *Synapse* **14**, 169 (1993).
24. R. H. Mach et al., *Pharmacol. Biochem. Behav.* **57**, 477 (1997).
25. M. Laruelle et al., *Neuropsychopharmacology* **17**, 162 (1997).
26. Materials and methods are available as supporting material on *Science* Online.
27. T. W. Robbins, *Psychopharmacology* **163**, 362 (2002).
28. J. Mukherjee et al., *Nucl. Med. Biol.* **26**, 519 (1999).
29. D. C. Roberts, M. E. Corcoran, H. C. Fibiger, *Pharmacol. Biochem. Behav.* **6**, 615 (1977).
30. S. B. Caine, G. F. Koob, *J. Exp. Anal. Behav.* **61**, 213 (1994).
31. H. O. Pettit, A. Ettenberg, F. E. Bloom, G. F. Koob, *Psychopharmacology* **84**, 167 (1984).
32. L. J. Vanderschuren, P. Di Ciano, B. J. Everitt, *J. Neurosci.* **25**, 8665 (2005).
33. M. G. Packard, B. J. Knowlton, *Annu. Rev. Neurosci.* **25**, 563 (2002).
34. H. H. Yin, B. J. Knowlton, B. W. Balleine, *Eur. J. Neurosci.* **19**, 181 (2004).
35. R. N. Gunn, A. A. Lammertsma, S. P. Hume, V. J. Cunningham, *Neuroimage* **6**, 279 (1997).
36. D. Martinez et al., *Neuropsychopharmacology* **29**, 1190 (2004).
37. G. R. Uhl, *Ann. N. Y. Acad. Sci.* **1025**, 1 (2004).
38. A. M. Persico, F. Bird, F. H. Gabbay, G. R. Uhl, *Biol. Psychiatry* **40**, 776 (1996).
39. S. B. Caine et al., *J. Neurosci.* **22**, 2977 (2002).
40. D. E. Comings, K. Blum, *Prog. Brain Res.* **126**, 325 (2000).
41. M. Shahmoradgoli Najafabadi et al., *Am. J. Med. Genet. Neuropsychiatr. Genet.* **134**, 39 (2005).
42. T. Pohjalainen et al., *Mol. Psychiatry* **3**, 256 (1998).
43. M. A. Nader et al., *Neuropsychopharmacology* **27**, 35 (2002).
44. M. S. Hooks et al., *J. Neurosci.* **14**, 6144 (1994).
45. B. J. Everitt, T. W. Robbins, *Nat. Neurosci.* **8**, 1481 (2005).
46. G. Paxinos, C. Watson, in *The Rat Brain in Stereotaxic Coordinates* (Academic Press, San Diego, CA, ed. 4, 1998), p. xxvi.
47. This research was supported by a joint award from the U.K. Medical Research Council (MRC) and the Wellcome Trust and by an MRC Pathfinder grant (G0401068) to J.W.D., B.J.E., and T.W.R. D.E.H.T. was supported by the Wellcome Trust. Y.P. was supported by a predoctoral Formación Investigadora scholarship from Generalitat de Catalunya. E.S.J.R. holds a Research Councils UK Academic Fellowship supported by the British Pharmacological Society Integrative Pharmacology Fund. E.R.M. was supported by a Gates Cambridge scholarship. We thank Merck, Sharp, & Dohme for originally donating the micro-PET scanner to Cambridge University.

---

# Reconstitution of DNA Segregation Driven by Assembly of a Prokaryotic Actin Homolog

Ethan C. Garner,[1,2,3] Christopher S. Campbell,[1,2,3] Douglas B. Weibel,[3,4] R. Dyche Mullins[1,2,3]*

Multiple unrelated polymer systems have evolved to partition DNA molecules between daughter cells at division. To better understand polymer-driven DNA segregation, we reconstituted the three-component segregation system of the R1 plasmid from purified components. We found that the ParR/*parC* complex can construct a simple bipolar spindle by binding the ends of ParM filaments, inhibiting dynamic instability, and acting as a ratchet permitting incorporation of new monomers and riding on the elongating filament ends. Under steady-state conditions, the dynamic instability of unattached ParM filaments provides the energy required to drive DNA segregation.

To ensure fidelity of gene transmission, DNA molecules must be evenly distributed among daughter cells before division. Eukaryotes harness the polymerization of tubulin to drive alignment and segregation of chromosomes (*1*); chromosome segregation in some eubacteria requires assembly of actin-like filaments (*2, 3*); and some extrachromosomal DNA elements have evolved their own polymer-based DNA segregation machinery (*4, 5*). Plasmid R1 is a large (100 kb), low–copy number plasmid with segregation machinery encoded by the *par* operon (*6, 7*). This operon is composed of three elements: *parC*, *parR*, and *parM* (*6*). *parM* encodes an actin-like protein that assembles into dynamically unstable filaments (*8*). *parR* encodes a protein that binds cooperatively to sequence repeats within *parC*, forming a complex that binds ParM filaments (*9*). It has been proposed that products of the *par* operon assemble into a bipolar spindle-like structure whose elongation drives plasmid segregation (*9*), but it is not yet

[1]Cellular and Molecular Pharmacology, University of California, San Francisco, CA 94158, USA. [2]UCSF/UCB Nanomedicine Development Center, San Francisco, CA 94158, USA. [3]Physiology Course, Marine Biological Laboratory, Woods Hole, MA 02543, USA. [4]Department of Biochemistry, University of Wisconsin, Madison, WI 53706, USA.

*To whom correspondence should be addressed. E-mail: dyche@mullinslab.ucsf.edu

known how these components assemble and how they convert the free energy of ParM polymerization into useful work.

By atomic structure, ParM is similar to actin (*10*), but by filament assembly dynamics, ParM is distinguished from actin by three important properties: (i) rapid, rather than slow, spontaneous nucleation; (ii) symmetrical, bidirectional elongation rather than polarized growth; and (iii) dynamic instability [the tendency to switch spontaneously (*11*) between phases of steady elongation and rapid shortening] rather than steady-state treadmilling (*8*). In vitro, the combination of these kinetic parameters results in a steady-state population of short (~1.5 μm) and unstable (lifetime ~20 s) ParM filaments (*8*).

To understand how ParR and *parC* harness filament assembly to segregate DNA, we purified all three components and tested their ability to self-assemble in vitro. We expressed and purified ParM and ParR proteins from *Escherichia coli* (fig. S1). We attached fluorescent (Cy3-labeled) DNA containing the *parC* sequence to 350-nm spherical beads. We then mixed the *parC*-coupled microspheres with ParR, added fluorescently labeled (Alexa 488) ParM, and induced filament assembly by adding adenosine triphosphate (ATP).

ParM filaments formed small radial arrays surrounding isolated *parC* beads (Fig. 1A), reminiscent of microtubule asters formed around isolated centrosomes (*12*). Aster formation required ATP, ParR (fig. S2A), and DNA containing the *parC* sequence (fig. S2B). Asters were dynamic, with filaments growing and shrinking from the surface of the bead, and grew to a maximum radius of 3 μm (Fig. 1B and movie S1), similar to the maximum lengths of individual ParM filaments in solution (*8*). In the presence of the nonhydrolyzable ATP analog adenylyl-imidodiphosphate (AMP-PNP), astral ParM projections grew much longer (Fig. 1C, fig. S3, and movie S2), indicating that the dynamic instability of ParM limited filament length even when one end of the filament was bound to the ParR/*parC* complex.

In addition to dynamic asters, ParM filaments also formed long, stable bundles connecting pairs of *parC* beads (Fig. 1, D to G), similar to bipolar structures previously observed in vivo (*7*). The bundles and attached beads moved as a single unit with fluid flow, indicating that ParM filaments were tightly attached to the ParR/*parC* complex. By electron microscopy (EM) we observed *parC* beads connected by ParM bundles of varying thickness. We traced individual filaments from one *parC* bead to the other (Fig. 1E), indicating that both ends of the ParM filament interacted with the ParR/*parC* complex. In time-lapse movies, the bivalently attached ParM bundles elongated at a constant rate, pushing *parC* beads in opposite directions (Fig. 1, D and F, and movies S3 and S4) over long distances (>120 μm). Thus ParM, ParR, and *parC* are sufficient to form a bipolar, DNA-segregating spindle. In addition,
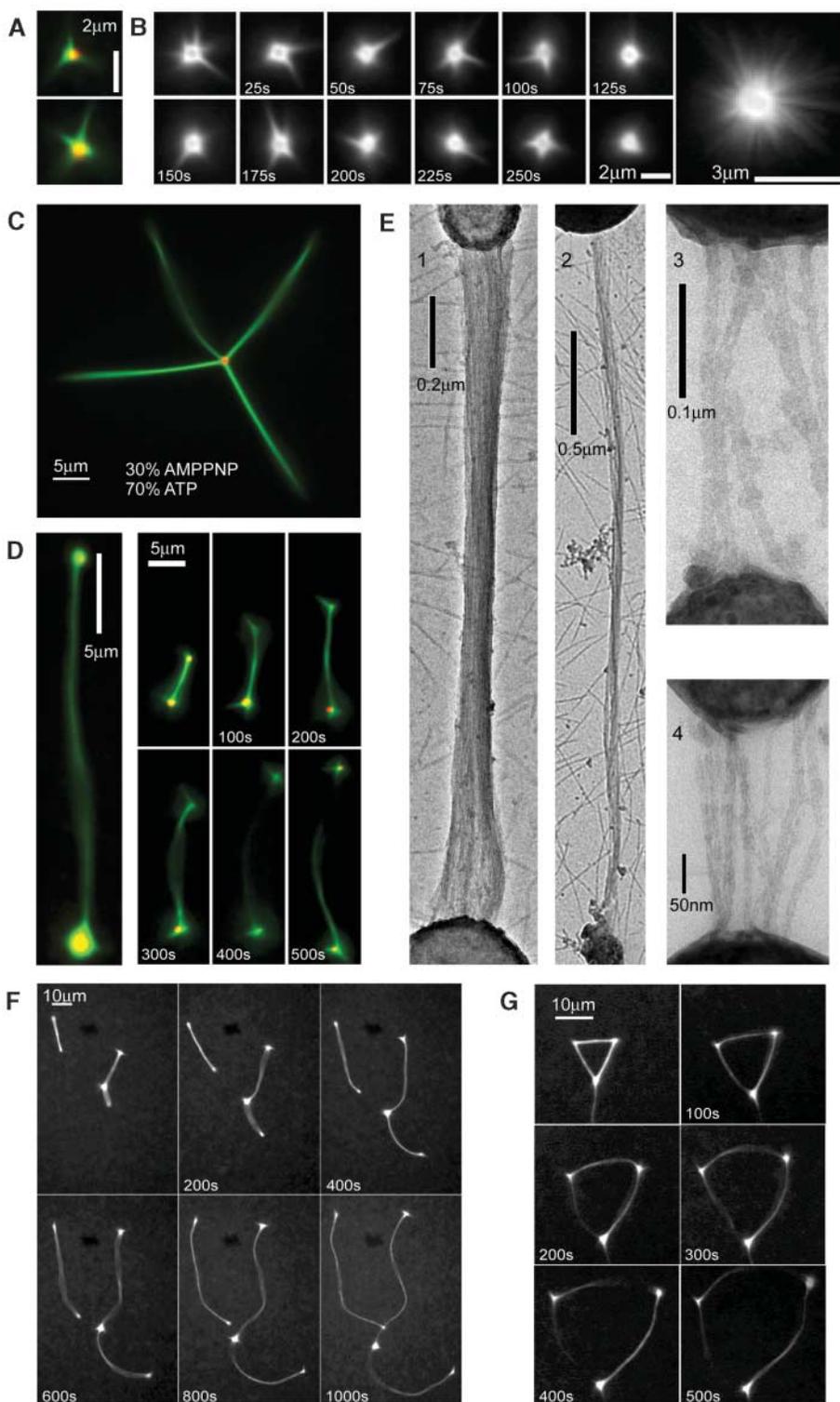


**Fig. 1.** In vitro reconstitution of the R1 plasmid spindle. (**A**) Individual ParR/*parC*-coated beads with radiating fluorescently labeled ParM asters (red, Cy3-labeled DNA; green, Alexa 488–labeled ParM). (**B**) Left: Time-lapse sequence of an Alexa 488–labeled ParM aster. Right: Maximum intensity projection of the time-lapse sequence, illustrating fall-off in fluorescence at 3 μm. (**C**) Inhibition of ParM dynamic instability with AMP-PNP produces substantially larger asters. (**D**) Two-color images and time-lapse sequence of bipolar ParM spindles segregating ParR/*parC*-coated beads. (**E**) Individual ParM filaments run from bead to bead, as shown by EM of negatively stained R1 spindles. (**F**) Time-lapse series of bipolar spindle elongation. (**G**) Elongation of a multipolar ParM structure.

multiple *parC* beads often interacted to form multipolar linear chains and polygons of ParM bundles (Fig. 1G and movies S5 and S6), structures that also expanded equilaterally as each bundle elongated at the same rate.

The fact that we observed long, stable ParM filaments only between pairs of *parC* beads argues that both ends of each filament are stabilized against catastrophic disassembly by interaction with the ParR/*parC* complex. This is supported by the observation of a "search-and-capture" (*13*) process of spindle formation: When two unconnected ParM asters come into proximity, they stabilize a filament bundle whose elongation pushes the asters apart (Fig. 2A, fig. S4, and movies S7 and S8). We tested whether bipolar attachment was required for stabilization by using laser irradiation to cut through ParM spindles. After cutting, both severed ends of the bundle depolymerized back to the *parC* beads (Fig. 2B, fig. S5, and movies S9 and S10). This requirement for bipolar stabilization of ParM spindles provides an explanation for the apparent plasmid counting observed in vivo, where ParM spindles occur only in cells containing two or more plasmids (*9*).

To determine whether the R1 spindle was sufficient to find the long axis of a bacterium-sized space, we assembled spindles in microfabricated channels of various shapes. Spindles always aligned with the long axis of the channel and pushed *parC* beads in opposite directions (Fig. 2C and movie S11), demonstrating that orientation of R1 spindles can occur without cellular landmarks. Spindles elongated freely until they encountered resistance. Elongation stalled at the ends of the channels and slowed at bends. Thus, the R1 spindle could find the long axis of a rod-shaped cell by a simple Brownian ratchet-type mechanism.

We next used photobleaching and speckle microscopy to determine where new ParM monomers incorporated into the R1 spindle. We first used low-intensity laser irradiation to photobleach pairs of reference marks onto elongating spindles (Fig. 3A, fig. S6, and movie S12). In all cases (*n* = 6), the distance between the two bleached marks did not change with time, whereas the distance between each mark and the nearest *parC* bead increased at a constant rate (Fig. 3B). We never observed recovery of fluorescence within a bleached zone, which suggests that no polymerization took place in the middle of the ParM bundle and that individual filaments did not slide past each other. Speckle microscopy (*14*) of elongating spindles indicated that monomers incorporated exclusively at the surface of *parC* beads (Fig. 3C and movies S13 and S14).

Interaction with the ParR/*parC* complex did not affect the rate of ParM filament growth. From the photobleaching and speckling experiments, we determined that filaments within a spindle elongate at a rate of $11.6 \pm 1.7$ monomers s$^{-1}$ ($n = 5$ ends). From the elongation rate and steady-state monomer concentration of 2.3 μM (*15*), we calculate a rate constant for elongation of bead-attached ParM filaments of 5 μM$^{-1}$ s$^{-1}$, identical to the rate constant for elongation of free ParM filaments (*8*).

In ParM mutants defective in ATP hydrolysis, the critical concentration for assembly is 0.6 μM (*8*). This is the free monomer concentration above which ATP ParM filaments elongate and below which they shorten. The critical concentration of adenosine diphosphate (ADP) ParM filaments is greater by a factor of more than 200 (>120 μM), and this nucleotide-dependent increase is the basis for dynamic instability of ParM filaments. At steady state, in the presence of ATP, the rate of filament nucleation is balanced by the rate of filament catastrophe, and the combination of growing and shrinking filaments produces a steady-
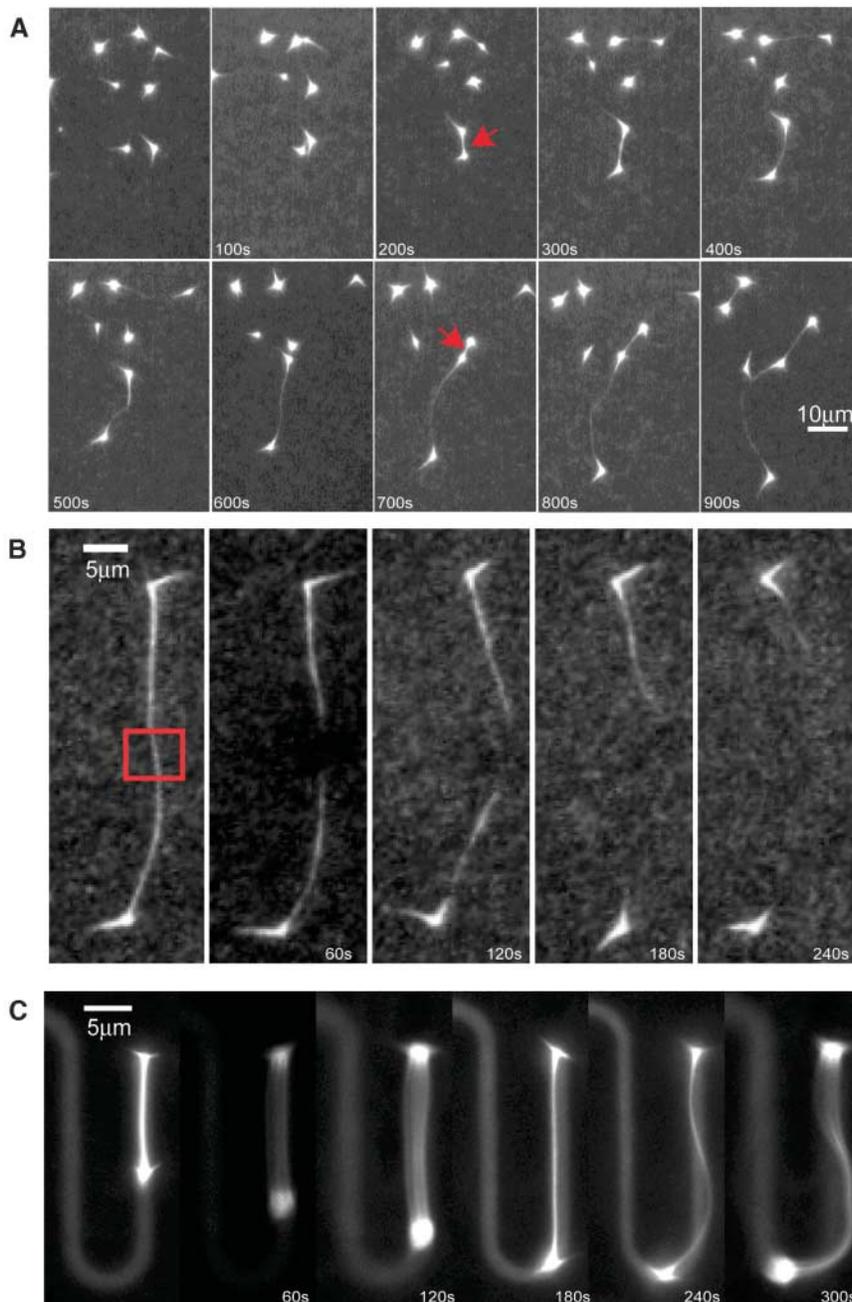


**Fig. 2.** ParM filaments are stabilized when bound at each end by the ParR/*parC* complex. (**A**) ParM spindles form by "search and capture." Sequence shows isolated ParM asters forming bipolar spindles that subsequently push the beads apart. Red arrows indicate capture events. (**B**) ParM filament bundles are stabilized a both ends by interaction with ParR/*parC* beads. Cutting a ParM spindle by laser irradiation (red box) results in depolymerization of severed ends. (**C**) The R1 spindle finds the long axis of a channel. Time-lapse sequence shows R1 spindles confined within a microfabricated channel.
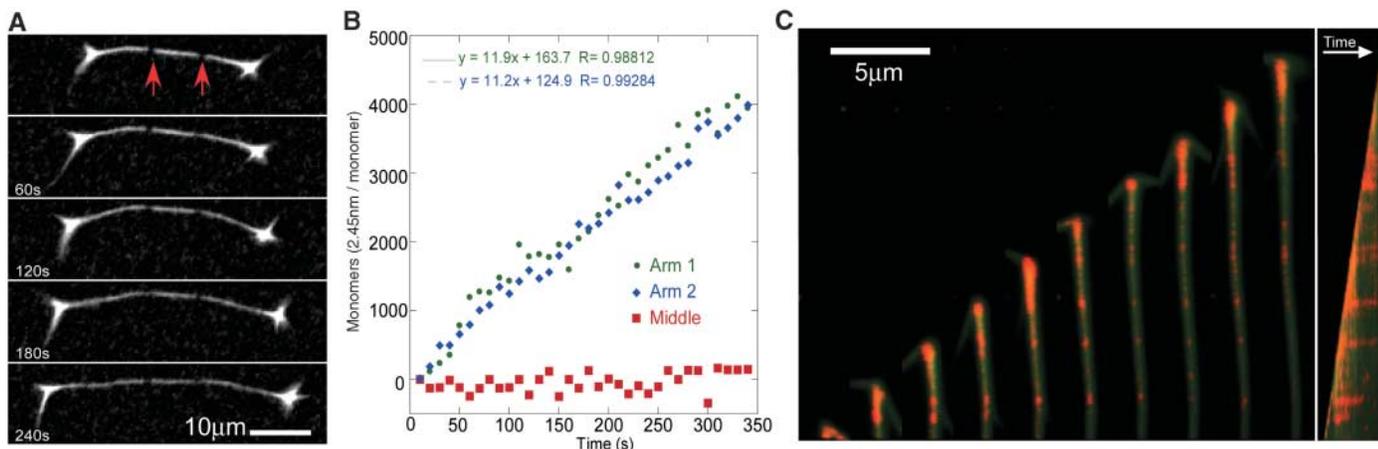
**Fig. 3.** R1 spindles elongate by insertion of ParM monomers at the ParR/*parC* complex. (**A**) Photobleaching (indicated by red arrows) of ParM spindles reveals symmetrical, bipolar elongation at the bead surface. (**B**) ParM spindles elongate at each end at the same rate as free filament ends. The distance between the two photobleached stripes or distance between the stripe and the bead in (A) was measured on a per-frame basis, and the change in distance was plotted against time. (**C**) By speckle microscopy, all new ParM monomers add to the spindle at the ParR/*parC* interface. Green, Alexa 488–ParM; red, rhodamine-ParM doped at 1:1000 to produce fluorescent speckles. Left: Time-lapse sequence of an elongating spindle end (80 s per frame). Right: Kymograph of the time-lapse sequence.

**Fig. 4.** Dynamic instability of free ParM filaments provides the energy for R1 spindle elongation. (**A**) The ParR/*parC* complex stabilizes ParM filaments down to the ParM-ATP critical concentration. Spindle assembly reactions were performed at the indicated concentrations of Alexa 488–labeled ParM. (**B**) By abolishing the difference in critical concentration between free and ParR/*parC*-bound ParM filaments, AMP-PNP eliminates sustained polymerization on ParR/*parC* beads. (**C**) Small amounts of ATP added into AMP-PNP restore sustained polymerization on ParR/*parC* beads. (**D**) Hydrolysis-dependent ParM tail elongation occurs specifically at filament ends bound to ParR/*parC* complexes and not at free filament ends. Assembly reactions as in (C) were initiated with Alexa 488–ParM (green); at indicated times, the reactions were spiked with Cy3-ParM (red). Results were visualized after 50 min. Two examples of each time point are shown. (**E**) Rates of ParM tail elongation scale with the fraction of hydrolyzable nucleotide. Reactions as in (C) were performed at various ATP/AMP-PNP ratios. The rate of tail elongation was plotted against the percent of ATP within the nucleotide mixture.
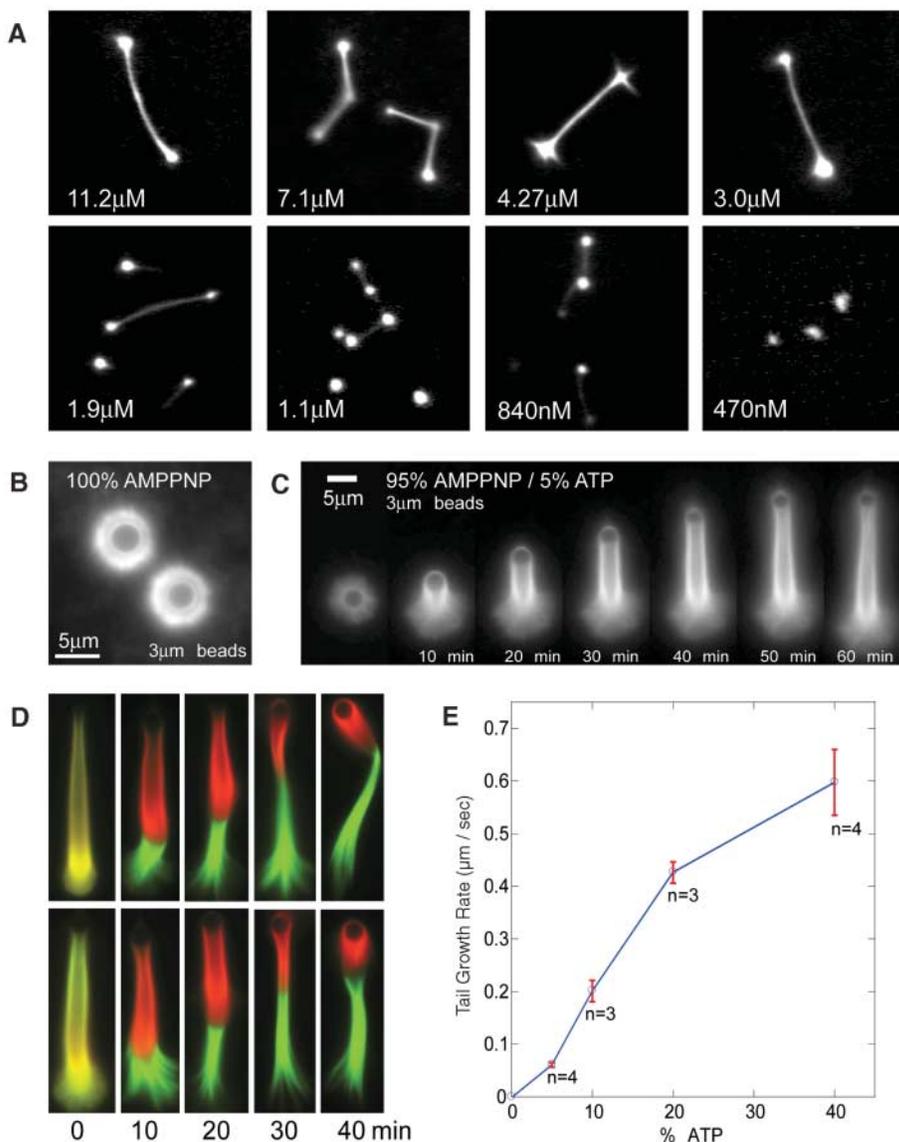
state monomer concentration of 2.3 μM. Beneath 2.3 μM, no filaments are detectable by fluorescence microscopy, fluorescence resonance energy transfer (FRET), or high-speed pelleting (*8*).

To determine how binding to the ParR/*parC* complex affects the critical concentration of ParM filaments, we investigated the concentration dependence of R1 spindle formation. At concentrations above 2.3 μM, ParM formed numerous dense and stable spindles connecting pairs of *parC* beads (Fig. 4A). Below 2.3 μM, ParM formed spindles between beads, but their frequency and lifetime decreased with decreasing ParM concentration. Below 0.6 μM, ParM failed to form any detectable spindles, even between *parC* beads in close contact. Thus, interaction with the ParR/*parC* complex stabilized ParM filaments down to, but not beneath, the ATP critical concentration of 0.6 μM, presumably because the ParR/*parC* complex simply inhibits dynamic instability.

One consequence of our results is that the energy to segregate *parC* beads must be supplied by dynamic instability of unattached ParM filaments. For polymerization to perform useful work, the monomer-polymer balance at the load must be kept away from equilibrium (*16*). We found that ParM filaments in the spindle are stabilized to the ATP critical concentration (0.6 μM) (Fig. 4A) yet elongate at a rate determined by the steady-state monomer concentration of 2.3 μM (Fig. 3B), a concentration that is maintained by dynamic instability of unattached ParM filaments (*8*).

To demonstrate this directly, we varied the energy difference between attached and unattached filaments by adding different ratios of ATP and AMP-PNP to our reconstituted DNA segregation system. In 100% AMP-PNP, the ParR/*parC*-attached and unattached filaments had the same critical concentration (0.6 μM), and the system quickly reached equilibrium (~2 min) with *parC* beads surrounded by a small, nondynamic shell of ParM filaments (Fig. 4B). Reestablishing an energy difference by adding small amounts of ATP produced sustained ParM polymerization at the bead surface. In 5% ATP and 95% AMP-PNP, slow-growing, stable, monopolar tails assembled on the surface of large *parC* beads, propelling them through the medium at a constant rate for up to 2 hours (Fig. 4C and movies S15 and S16). By using two colors of labeled ParM, added at different times (Fig. 4D), we found that filament elongation occurred exclusively on ParR/*parC* associated ends and not on free ends. Hence, the unattached filament ends are at steady state, whereas ParR/*parC*-associated ends elongate in a hydrolysis-dependent manner. The elongation rate of stabilized tails increased with the proportion of hydrolyzable ATP (Fig. 4E), demonstrating that the energy difference driving bead motility was proportional to the amount of hydrolysis-capable monomer that could be stabilized by the ParR/*parC* complex.

In response to evolutionary pressure, the R1 plasmid has evolved a self-contained, three-component system to ensure its segregation. All key functions of the R1 spindle require dynamic instability of ParM filaments. Dynamic instability enables unbound filaments to turn over without disassembly factors (*8*). Filaments stabilized at one end by ParR/*parC* can search for additional plasmids (fig. S8 and movie S17); filaments bound at both ends are stabilized against dynamic instability, forming a productive spindle. Finally,

the dynamic instability of unbound filaments provides the excess monomer to drive elongation of the stabilized filaments within the spindle.

### References and Notes

1. S. Inoue, H. Sato, *J. Gen. Physiol.* **50** (suppl.), 259 (1967).
2. Z. Gitai, N. A. Dye, A. Reisenauer, M. Wachi, L. Shapiro, *Cell* **120**, 329 (2005).
3. T. Kruse *et al.*, *Genes Dev.* **20**, 113 (2006).
4. K. Gerdes, J. Moller-Jensen, R. Bugge Jensen, *Mol. Microbiol.* **37**, 455 (2000).
5. G. E. Lim, A. I. Derman, J. Pogliano, *Proc. Natl. Acad. Sci. U.S.A.* **102**, 17658 (2005).
6. K. Gerdes, S. Molin, *J. Mol. Biol.* **190**, 269 (1986).
7. J. Moller-Jensen, R. B. Jensen, J. Lowe, K. Gerdes, *EMBO J.* **21**, 3119 (2002).
8. E. C. Garner, C. S. Campbell, R. D. Mullins, *Science* **306**, 1021 (2004).
9. J. Moller-Jensen *et al.*, *Mol. Cell* **12**, 1477 (2003).
10. F. van den Ent, J. Moller-Jensen, L. A. Amos, K. Gerdes, J. Lowe, *EMBO J.* **21**, 6935 (2002).
11. T. Mitchison, M. Kirschner, *Nature* **312**, 237 (1984).
12. M. Moritz *et al.*, *J. Cell Biol.* **130**, 1149 (1995).
13. T. E. Holy, S. Leibler, *Proc. Natl. Acad. Sci. U.S.A.* **91**, 5682 (1994).
14. C. M. Waterman-Storer, A. Desai, J. C. Bulinski, E. D. Salmon, *Curr. Biol.* **8**, 1227 (1998).
15. See supporting material on *Science* Online.
16. J. A. Theriot, *Traffic* **1**, 19 (2000).
17. We thank O. Akin and M. Quinlan for assistance with bead motility assays, Q. Justman and A. Murray for helpful discussions, and S. Layer for continued advice and inspiration. Supported by NIH grants RO1GM61010 and R01GM675287, the Sandler Family Supporting Foundation, and the UCSF/UCB Nanomedicine Development Center (R.D.M.).

# Multiple Functions of the IKK-Related Kinase IKKε in Interferon-Mediated Antiviral Immunity

Benjamin R. tenOever,[1] Sze-Ling Ng,[1] Mark A. Chua,[2,3] Sarah M. McWhirter,[1] Adolfo García-Sastre,[2,4] Tom Maniatis[1]*

IKKε is an IKK (inhibitor of nuclear factor κB kinase)–related kinase implicated in virus induction of interferon-β (IFNβ). We report that, although mice lacking IKKε produce normal amounts of IFNβ, they are hypersusceptible to viral infection because of a defect in the IFN signaling pathway. Specifically, a subset of type I IFN-stimulated genes are not activated in the absence of IKKε because the interferon-stimulated gene factor 3 complex (ISGF3) does not bind to promoter elements of the affected genes. We demonstrate that IKKε is activated by IFNβ and that IKKε directly phosphorylates signal transducer and activator of transcription 1 (STAT1), a component of ISGF3. We conclude that IKKε plays a critical role in the IFN-inducible antiviral transcriptional response.

Activation of innate immunity by virus infection begins with type I IFNα and IFNβ gene expression followed by induction of the Janus kinase–signal transducer and activator of transcription (JAK-STAT) pathway, leading to the expression of a large family of IFN-stimulated genes (ISGs) (*1*). The initial response is triggered by pattern recognition receptors that bind to virus-specific molecular signatures and activate latent kinase complexes such as the stress-activated protein kinases (c-Jun N-terminal kinase and p38), the IKK complex (IKKα/IKKβ/IKKγ), and the IKK-related kinases TANK-binding kinase 1 (TBK1) and IKKε [also called IKKi (*2*)] (*3*). These kinases coordinate the assembly of the IFNβ enhanceosome, a multisubunit complex composed of the transcription factors ATF2 (activating transcription factor 2)/cJun, NFκB, and interferon regulatory factors 3 and 7 (IRF3 and IRF7) (*3*). IFNβ induces dimerization of the type I IFN receptor and activates the associated kinases tyrosine kinase 2 (TYK2) and JAK1 (*1*), leading to the tyrosine phosphoryl-

[1]Department of Molecular and Cellular Biology, Harvard University, 7 Divinity Avenue, Cambridge, MA 02138, USA. [2]Department of Microbiology, Mount Sinai School of Medicine, One Gustave L. Levy Place, Box 1124, New York, NY 10029, USA. [3]Microbiology Graduate School Training Program, Mount Sinai School of Medicine, One Gustave L. Levy Place, Box 1124, New York, NY 10029, USA. [4]Emerging Pathogens Institute, Mount Sinai School of Medicine, One Gustave L. Levy Place, Box 1124, New York, NY 10029, USA.

*To whom correspondence should be addressed. E-mail: maniatis@mcb.harvard.edu